Chapter 13
A Semi-active Control System for Wind Turbines

N. Caterino, C.T. Georgakis, F. Trinchillo and A. Occhiuzzi

Abstract A semi-active (SA) control system based on the use of smart magnetorheological (MR) dampers to control the structural response of a wind turbine is proposed herein. The innovative approach is based on the implementation and use of a variable-properties base restraint. This is able to modify in real time its mechanical properties according to the instantaneous decision of a given control logic, the latter addressed to control one or more structural response parameters. The smart base restraint is thought to be a combination of a smooth hinge, elastic springs, large-scale adjustable MR dampers, and a control algorithm that instantaneously commands the latter during the motion, making them to modulate the reactive force as needed to achieve the performance goals. The design and operation of such a system are shown with reference to a case study consisting of an almost 100 m tall wind turbine, realized in a 1/20 scale model at the Denmark Technical University (DTU). Shaking table tests have been performed under the action of two different types of wind loads and by using two purposely written control logics, highlighting the high effectiveness of the proposed SA control technique and encouraging to further investigate in such direction.

Keywords Semi-active control · Wind turbine · Magnetorheological damper · Smart material · Control algorithm

N. Caterino (✉) · F. Trinchillo · A. Occhiuzzi
University of Naples "Parthenope", Naples, Italy
e-mail: nicola.caterino@uniparthenope.it

F. Trinchillo
e-mail: francesco.trinchillo@uniparthenope.it

A. Occhiuzzi
e-mail: antonio.occhiuzzi@uniparthenope.it

C.T. Georgakis
Technical University of Denmark (DTU), Copenhagen, Denmark
e-mail: cg@byg.dtu.dk

13.1 Introduction

In the last years the need for optimization procedures to design higher and higher wind turbines, even offshore, in a cost-effective way and of control techniques to reduce the wind-induced structural demand has definitely grown. Most of the scientific literature on this topic is related to passive control strategies, often based on the use of tuned mass or tuned liquid dampers.

Herein, the possible use of a semi-active (SA) control technique is investigated, based on the use of magnetorheological (MR) dampers, also performing large-scale shaking table tests. Previous researches on SA control of wind turbines are not much based on numerical simulations.

Kirkegaard et al. [1] for the first time explored the possibility of using MR dampers to control a wind turbine, numerically evaluating their effectiveness when driven by a classical optimal clipped control algorithm. The proposed idea was pioneering and, also because of this, it results to be very interesting, even if difficult to be implemented in a real case. As a matter of a fact, the authors consider the installation of an MR device at the base of the tower, in vertical position, so as to be able to be solicited by relative vertical displacements induced by the top movement of the turbine to which the damper should be mechanically connected. Also an experimental test model has been built by the said authors, even if adopted for passive tests only (constant voltage fed to the MR damper at the maximum level—"passive-on" condition). The wind turbine model was a 3 m high steel frame with a 200 kg top mass. The MR damper was connected to the shaking table and to the top of the frame structure by a steel bar designed so as to avoid buckling. Comparing numerical (SA) and experimental (passive) results in terms of top displacement, appreciable improvements in the SA strategy are highlighted by the authors.

Karimi et al. [2] and Luo et al. [3–5] showed the effectiveness of SA control for floating wind turbines by using tuned liquid column dampers (TLCD). This kind of device is generally used as a passive damper, even if it may turn into an SA damper with the addition of a controllable valve. With a control logic based on an H_∞ feedback methodology, the authors proposed to adopt the orifice opening according to the structure response and loading conditions. Luo et al. also explored the possibility of using MR fluids within the TLCD, rather than a common viscous fluid, so leading to a "smart" TLCD [6, 7]. The numerical simulations reported in the above papers show that this kind of control strategy may lead to a strong reduction of the top displacement.

Arrigan et al. [8] considered SA tuned mass dampers (STMD) to control wind turbine blades in flapwise vibrations. Four STMDs were added to the wind turbine numerical model, one to each blade tip and one at the nacelle to control the response of each component. Simulations made by the authors showed a significant reduction in displacement response of the system for turbulent wind loading. A successful response reduction under a steady wind load was demonstrated.

Rodríguez et al. [9] explored the possibility to use passive or SA dampers in a toggle brace assembly integrated within the hollow column of a wind turbine tower. They evaluated the effectiveness of this control technique in terms of reduction of base bending moment for extreme and fatigue loads. Different configurations of such system have been compared by authors, each defined by a given number, position, and inclination of the devices in both the horizontal and vertical planes. The best option leads to a reduction in the moment demand at the base of the tower up to 20 % in extreme cases and around 10 % in fatigue.

The basic idea for the SA control technique proposed herein consists in using the smart MR devices so as to realize a time-variant base restraint, whose "stiffness" is in real time driven by a purposely written control logic. The latter instantaneously takes decision and calibrates MR dampers to reduce the bending stress at the base of the tower, secondarily to bound the top displacement within acceptable limits so as to avoid significant, detrimental second order effects.

This strategy has been experimentally assessed at the shaking table facility of the Denmark Technical University (DTU) in Copenaghen, where the present control concept was initially conceived. Two different base accelerograms were imposed for the tests, equivalent to an extreme short operating gust and a longer high velocity wind buffeting, respectively. Moreover, two distinct control algorithms have been designed and adopted for the tests, different in the way they approach the problem. The first is inspired to the eigenstructure selection technique [10, 11] and is addressed to significantly increase the modal damping ratios, and to make the fundamental mode similar to a rigid rotation of the tower around the base hinge. The second algorithm follows a more physical approach, being designed to bound the stress at the base and, as a secondary objective, the top displacement demand within given limits.

All the performed tests highlight the effectiveness of the proposed control technique in reducing the stress demand at the base, this at the cost, in the worst case, of a slight increase in top displacement.

13.2 Basic Idea of the Semi-active Control Strategy

The realization of a time-variant restraint at the base of the tower exploiting the potential of smart dampers is the basic idea herein proposed to reduce wind-induced structural demand to high-rise turbines. This is roughly described in Fig. 13.1, where the original wind turbine is modeled as a single degree of freedom dynamic system with top mass, stiffness, and inherent damping equal to m, k_T and c_T respectively, fully restrained at the base (Fig. 13.1a). The idea is replacing this perfectly rigid base restraint with a controllable one that, during the motion, can be instantaneously made more or less "stiff" depending on what is more beneficial in terms of reducing the structural demand. Figure 13.1b schematically describes a possible way to materialize this concept, by installing at the base of the tower a smooth hinge, a rotational spring (stiffness k_ϕ), and a rotational variable damper

Fig. 13.1 Basic idea of SA control of a wind turbine via MR dampers
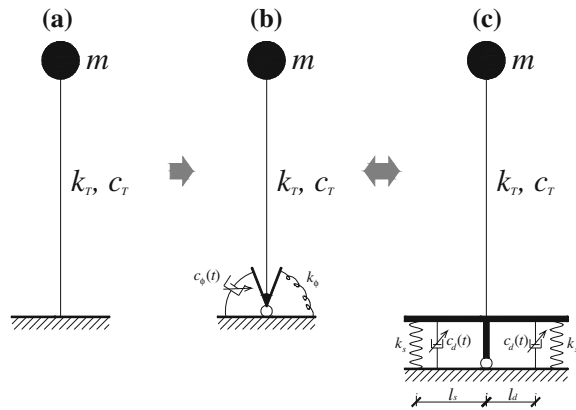
(damping constant c_ϕ, variable in time) externally driven in real time by a control algorithm. The same concept can be practically implemented by means of two vertical linear springs (k_s) installed at a given distance (l_s) from the hinge and two vertical variable dampers (c_d), each placed at the distance l_d from the hinge (Fig. 13.1c).

MR dampers are suggested to be adopted as variable devices within this setup. At macro scale, MR fluids behave as semi-solid bodies as far as the shear stress does not exceed a threshold, whose value depends on the intensity of the magnetic field the fluid is immersed in, the latter depending in turn on the current intensity in coils placed around the fluid. This behavior is associated to the nature of the fluid, a suspension of micron-sized magnetizable particles. Upon application of a magnetic field, particles align and form fibrous aggregates that generate orders-of-magnitude viscosity changes within characteristic times of milliseconds.

When the base damping is set to a low value, the tower is able to relax, hence to convert its potential energy into kinetic energy and to reduce the bending moment at the base. Thus the SA base system implies stress reduction, even at the cost of a possible increase of top displacement, which has to be bounded within certain limits to control the top displacements. The springs allow to reset the tower to the initial position at the end of a severe wind-induced excitation.

This idea has been physically realized and tested at the laboratory of the DTU (Copenaghen) by using prototype MR dampers provided by Maurer Söhne (Germany). The results gained from this campaign will be presented and discussed in the following sections.

13.3 Experimental Setup

A 3 MW wind turbine with horizontal power transmission axle has been assumed as reference structure for the experimental campaign performed at the DTU laboratory (Fig. 13.2). The tower is 102.4 m tall, made of steel Q345 (modulus of
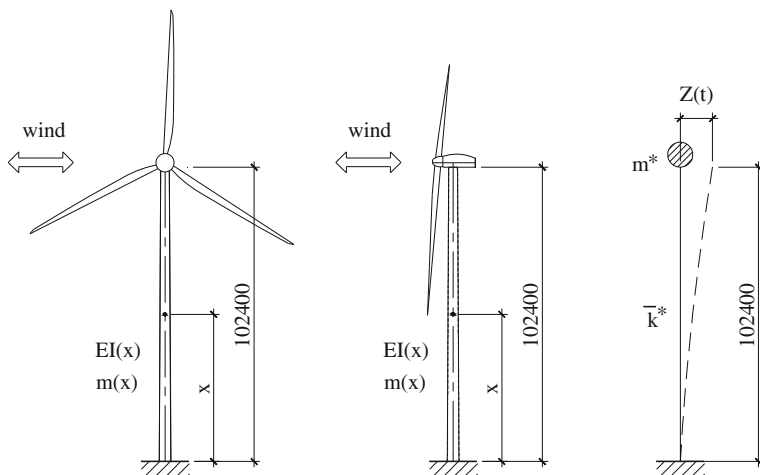
Fig. 13.2 Structural model of the reference wind turbine [12]. Dimensions in milimeters

elasticity 206,000 MPa, Poisson ratio 0.3, yielding stress 345 MPa), with a variable hollow circular cross section with external diameter variable from 2.30 m (top) to 4.15 m (bottom). The weight of the tower, including the flanges and internals, is 3,713 kN (body) and 1,210 kN (nacelle, including the rotor blades). Chen and Georgakis [12, 13] showed the equivalence, from a dynamic point of view, of this structure with a single degree of freedom (DOF) system made up of a tapered tubular cantilever beam with a concentrated mass at the top. In the same studies, the development of a 1/20-scale model of the prototype structure is presented. This test model is characterized by a 5.12 m high vertical tube with uniform cross section $\Phi133/4$ (i.e., a hollow circular one with 133 mm of external diameter and 4 mm in thickness), chosen according to the principle of the equivalent flexural stiffness, with a lumped mass of 280 kg placed at the top (Fig. 13.3).

The base of the model is realized so as to be stiff enough, by means of two parallel, horizontal steel C profiles (UPN 240 cross section) whose top and bottom flanges are firmly bolted to stiff, horizontal steel plates. It is connected in the middle to the shaking table through a cylindrical steel hinge, with interposed a small, stiff steel frame. On both sides of the base, one cylindrical spring (89 kN/m stiff) and one MR damper (described in the next section) are installed.

The shaking table facility used for the test consists of a platform made of 20 mm thick aluminum plates 1.5×1.5 m in plan. The table can be moved in a single horizontal direction by a 100 kN hydraulic actuator MTS 244.22. Stiffness grid plates of 300×300 mm are welded to the top and bottom plates. Furthermore, in the areas where the forces are transmitted, additional stiffeners have been added.
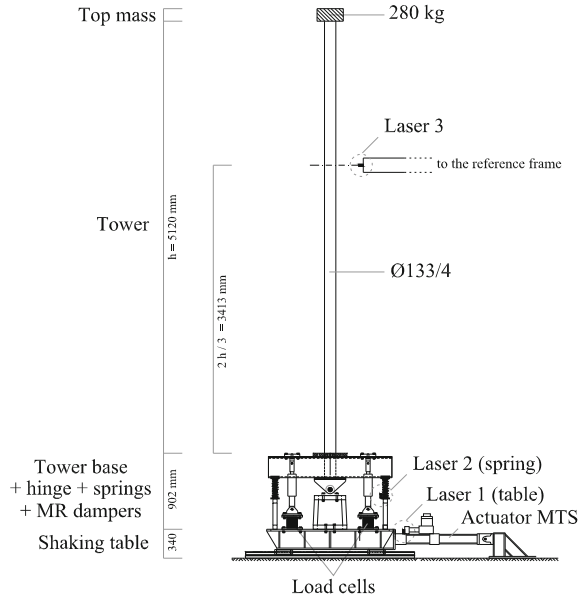
Fig. 13.3 Experimental setup

Figure 13.3 shows the overall experimental setup, whereas Fig. 13.4 includes a detail of the base to better understand how the smart base restraint has been realized. Such figures also report the type and position of all the transducers adopted, whereas further details are given in the following sections. Some photographs of the setup are given in Fig. 13.5.

13.3.1 Electronic Equipment and Transducers

The electronic equipment adopted for the experimental activity on the wind turbine model can be formally distinguished into two parts: conventional tools for structural laboratory tests and an extra-equipment properly required for SA control by means of two MR dampers.

The position of the transducers belonging to the first group is shown in Figs. 13.3 and 13.4. The horizontal displacements of the shaking table were measured through a laser transducer supported by a steel stick (WayCon laser, model LAS-T-500, range of measure 50–550 mm). The same kind of laser transducer was located at 2/3 of total height of the tower and fixed to an external wood stick to measure the absolute horizontal displacement of that section. The axial displacements of springs were measured by a third laser transducer attached on the steel plate where one of the 2 springs (the one closer to the actuator) is installed (WayCon laser, model LAS-T-250, range of measure 50–300 mm). Rotation of the base and axial displacements of MR dampers have been calculated
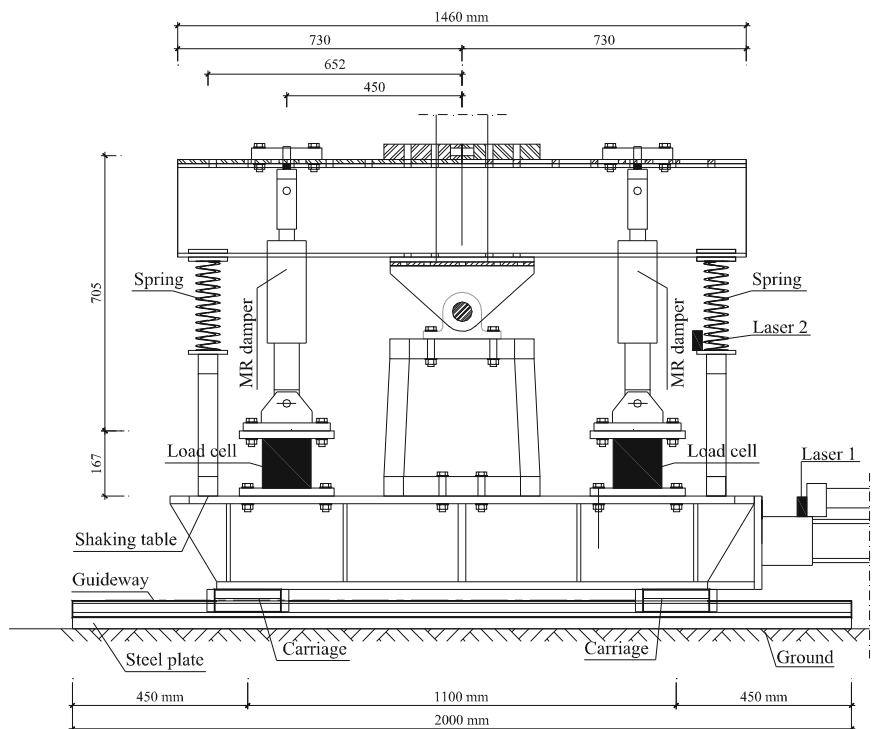
Fig. 13.4 Detail of the base of the mock-up structure

online, by considering the reciprocal position of cylindrical hinge, dissipators, and springs (Fig. 13.4). Two load cells mounted under each MR device allowed to measure the reacting forces (AMTI load cells, model MC5-5000, range ±22 kN). It is worth noting that base stress and top displacement have been calculated online from the above-mentioned available displacement measures, being the stress of steel well below the yielding value.

The additional electronic equipment used to drive the SA tests include (Fig. 13.6):

1. No. 2 power supplies type BOP (Bipolar Power Supply) provided by Kepco Inc. (New York, USA), model 50–4 M, maximum power output of 200 W, maximum input power of 450 W, power source-power sink capabilities in the range ±50 V (voltage) and ±4 A (current); commanded from a remote location (PC) through a voltage signal in the range 0–10 V, with alternative operations as voltage driver (control loop gain 5.0 V/V) or as current driver (control loop gain 0.4 A/V);
2. No. 1 embedded controller National Instruments PXI-8196 RT, high-performance platform for testing in real time;

Fig. 13.5 Photograph of the structural model installed at the DTU laboratory. Overall view (**a**), *lateral* (**b**) and *front* (**c**) view of the base
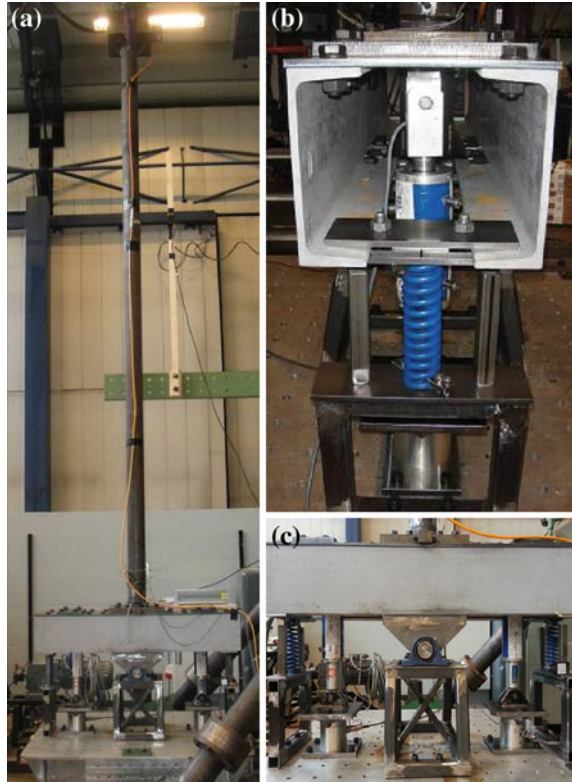
3. No. 2 data acquisition boards National Instruments PXI-6259, multi-function high-speed, optimized for high accuracies and speed of acquisition (up to 2,800 kHz), 8-channel analog inputs, 4 analog outputs (in the range ±10 V), 16 bits of resolution;

4. No. 1 digital multimeter National Instruments PXI-4065, 6 ½-digit for high speed measuring of voltage, current and resistance;

5. No. 2 connector blocks National Instruments BNC-2110;

6. No. 1 voltage attenuator module (10 to 1) National Instruments SCC-A10, dual channel, with voltage inputs up to ±60 V ("C" in Fig. 13.6);

7. No. 1 capacitance of 1.0 μF needed to stabilize the current loop ("A" in Fig. 13.6);

8. The software environment NI Labview Professional Development System ("B" in Fig. 13.6);

9. Real time operating system labview by NI for testing in real time;

10. No. 1 chassis national instruments able to host components 2, 3, 4 ("D" in Fig. 13.6).
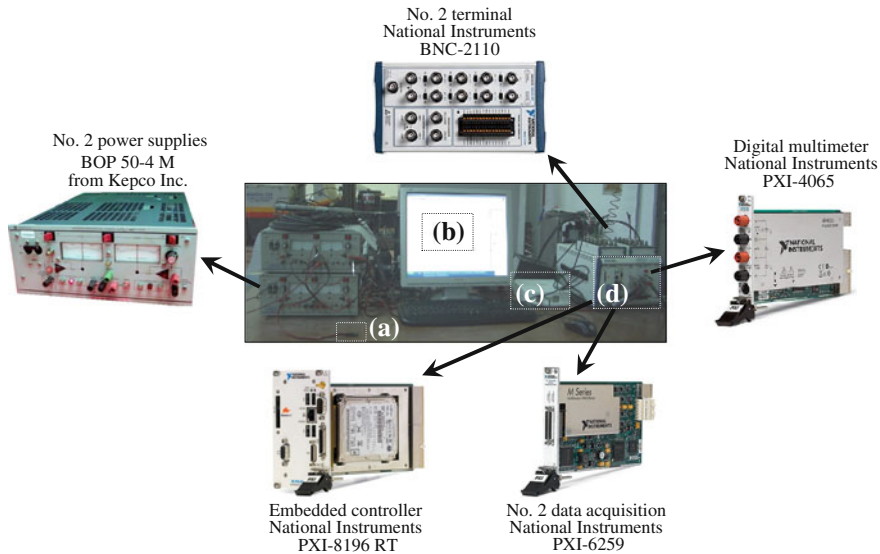
No. 2 terminal
National Instruments
BNC-2110

No. 2 power supplies
BOP 50-4 M
from Kepco Inc.

Digital multimeter
National Instruments
PXI-4065

(b)

(c)   (d)

(a)

Embedded controller
National Instruments
PXI-8196 RT

No. 2 data acquisition
National Instruments
PXI-6259

Fig. 13.6 Electronic equipment for acquisition and semi-active control

13.4 Magnetorheological Dampers

The devices adopted for the tests were two full-scale prototype SA MR dampers (Fig. 13.7) designed and manufactured by the German company Maurer Söhne. The overall dimensions of each device are 675 mm (length) $\times$ 100 mm (external diameter), with a mass of about 16 kg. A maximum force of about 30 kN can be developed along the longitudinal axis, whereas the presence of special spherical pin joints at both ends prevents the rise of bending, shear, and torsional moment in the piston rod. The dampers have a stroke of ± 25 mm. The external diameters of the piston head and of the piston rod are 100 and 64 mm, respectively. A magnetic circuit composed of coils, in series with a global resistance of 3.34 Ω, can generate the magnetic field in the device. The current in the circuit can be provided in the range $0 \div 4$ A.

The MR dampers were first experimentally tested by using a self-balanced testing apparatus (Fig. 13.8). Some general information is provided herein. Further details can be found in [14].

Figure 13.9 shows the results of four "passive" (constant value of current) tests done imposing the same harmonic displacement at the mobile end of the device (frequency 1.5 Hz, amplitude 20 mm) with four different current levels (0.0, 0.9, 1.8, and 2.7 A).

The force-displacement and force-velocity cycles clearly show how the damper's mechanical behavior strongly depends on the magnetic field inside the device and, in turn, on the current intensity inside the coils. In particular, the maximum

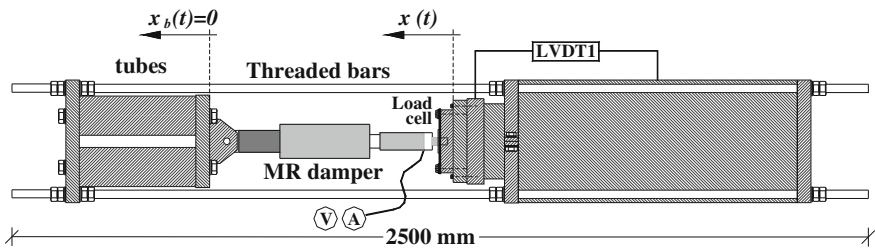**Fig. 13.7** One of the two prototype MR dampers

Fig. 13.8 Photograph and sketch of the experimental apparatus
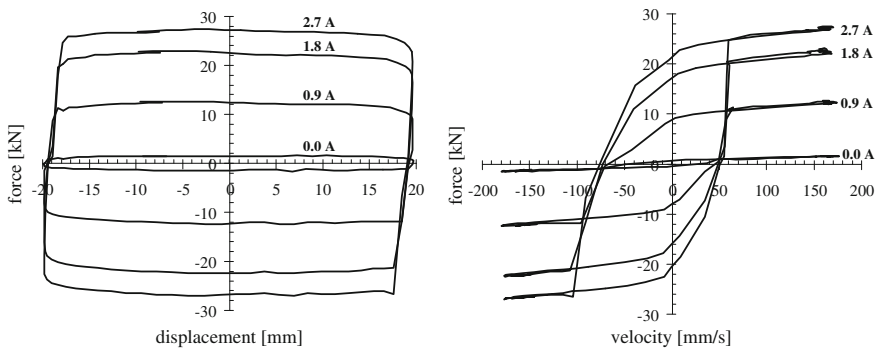

Fig. 13.9 Experimental response of one MR damper under 1.5 Hz, ±20 mm harmonic displacement
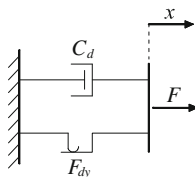
Fig. 13.10 Bingham model for MR dampers

measured force turned out to be approximately 2 kN when no current was given to the damper and to achieve the values 12, 22, and 27 kN when the feeding currents 0.9, 1.8, and 2.7 A were provided, respectively.

The force-displacement loops look substantially like a superposition of a viscous and friction-like behavior (Fig. 13.10), both depending on the magnitude of the current intensity [15]. This behavior, based on the properties of Bingham solids [16], can be analytically described as in Eq. 13.1 where $\dot{x}$ is the relative velocity between the damper's ends, C_d the viscous damping, F_{dy} the plastic threshold, both functions of the applied magnetic field and, in turn, of the intensity of current i:

$$F = C_d(i) \cdot \dot{x} + F_{dy}(i) \cdot \text{sgn}(\dot{x}). \tag{13.1}$$

The relationships C_d (i) and F_{dy} (i) have been found by interpolating by a second order polynomial function the experimental data (Eqs. 13.2–13.3, where A, kN, s, m are the adopted units of measure) and are graphically described in Fig. 13.11.

$$C_d(i) = -1.870\,i^2 + 13.241\,i + 6.851 \tag{13.2}$$

$$F_{dy}(i) = -1.952\,i^2 + 13.962\,i + 0.181. \tag{13.3}$$

The curves in Fig. 13.11 show an asymptotic trend of the MR effect associated to magnetic saturation of the MR fluid.

A detailed report of the response time analysis of such prototype MR dampers based on the above-mentioned experimental data is also presented in [17]. The promptness turned out to be mainly related to the electric part of the control chain. "Power source—power sink" capabilities resulted to be crucial to make the device able to operate in real time. Furthermore, current-driven operations rather than voltage-driven resulted to be strongly recommended to dramatically shorten control lead times. In voltage-driven operations, the power supply provides a fixed voltage and the current slowly modifies until it reaches the desired value, corresponding to the ratio voltage/resistance. In current-driven operations, the power supply provides a fast changing voltage spike so as to quickly modify the current inside the damper, causing in turn a fast change in the mechanical behavior of the damper. If the current must be increased, the power supply provides for a short
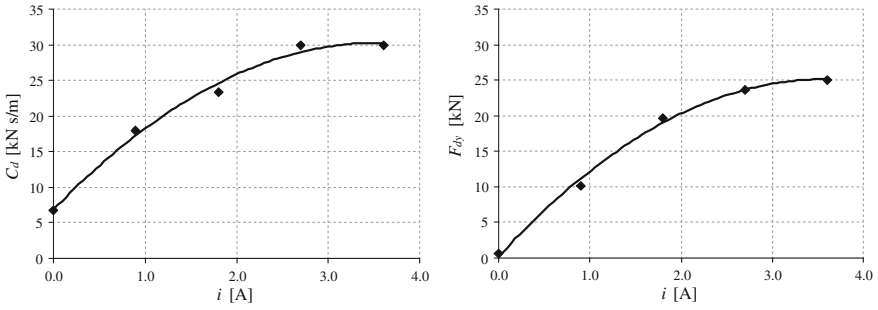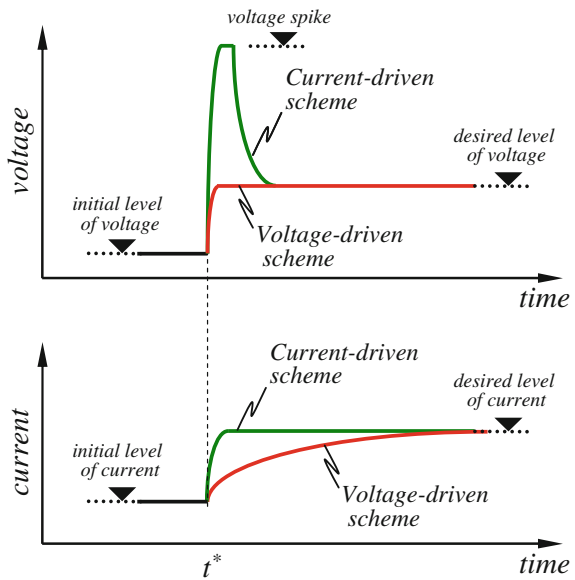
Fig. 13.11 Bingham model parameters for the prototype MR dampers

Fig. 13.12 Qualitative trends in current and voltage for two alternative approaches to control MR dampers (t^* is the instant of command)

period a voltage spike and then sets the voltage to the reference value, whereas if the current must be decreased, a negative spike of voltage is issued.

Figure 13.12 qualitatively shows what happens to voltage and current into an MR damper when the two approaches are adopted, showing the delay with which the current (and the corresponding magnetic field) reaches the desired value when a voltage-based approach is adopted.

It is experimentally demonstrated that using current-based strategy for control and an appropriate and suitably tuned electric hardware, the response time of the above-mentioned prototype SA MR dampers can be comfortably bounded to 8–10 ms.

Recently, these smart devices has been successfully used also in a wide experimental campaign to SA control earthquake-induced vibrations of a 3D large scale steel structure installed on a shaking table facility at the University of Basilicata (Italy), allowing a comparison of four different control algorithms and resulting very effective in reducing structural response [18]. Herein, the high versatility of SA control strategies based on MR dampers is demonstrated.

13.5 Control Algorithms

The first controller adopted for the shaking table tests is based on the eigen-structure selection theory [10, 11]. It is a full-state feedback algorithm relying on real-time definition of a desired control force and on the ability of the SA reacting forces to mimic it during the motion. The second algorithm instead is designed to bound the stress at the base within acceptable, given limits, also controlling the top displacement to avoid the occurrence of significant second order effects.

A simplified, lumped-mass model of a wind turbine tower mounted on a rotating base is shown in Fig. 13.13. The base is linked to the ground through two elastic elements (springs), two SA MR dampers and a hinge, as described in Sect. 13.2. In the figure:

h	is the height of the tower;
m_1-m_r	are the lumped masses of the model;
k_1-k_r	are the stiffnesses associated to the various DOFs;
c_1-c_r	are the viscous damping coefficients associated to the various DOFs;
α	is the rotation of the base;
$\delta_0 = \alpha \times h$	is the corresponding rigid displacement of the top of the tower;
δ_1-δ_r	are the elastic displacements of the lumped masses;
k_s	is the stiffness of each base spring;
f_{d1}-f_{dm}	are m independent control forces available;
l_s	is the distance between each spring and the hinge;
l_d	is the distance between each SA MR damper and the hinge.

The equations of motion of the $n = r + 1$ DOFs system in the absence of any external disturbance are

$$\mathbf{M}\ddot{\boldsymbol{\delta}} + \mathbf{C}\dot{\boldsymbol{\delta}} + \mathbf{K}\boldsymbol{\delta} = -\mathbf{P}\mathbf{f}_d \qquad (13.4)$$

where $\mathbf{M}$, $\mathbf{C}$ and $\mathbf{K}$ are, respectively, the mass, damping, and stiffness matrices, $\mathbf{P}$ is the $n \times m$ allocation matrix of the control forces f_{di} collected in the control vector $\mathbf{f}_d$ and $\boldsymbol{\delta} = [\delta_0\ \delta_1\ \ldots\ \delta_r]^T$ is the vector collecting the DOFs, whose components are scalar functions of time. However, the dependency from time will be explicitly written only when needed.

Fig. 13.13 Lumped-mass
structural model of a wind
turbine
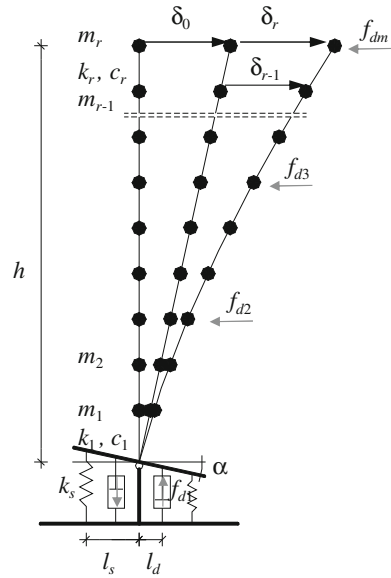
When the control forces are not present, in the typical hypothesis of neglecting
damping, the eigenvector analysis of the system described by Eq. 13.4, namely the
search for solutions of the equation

$$\omega^2 \mathbf{I} - \mathbf{M}^{-1}\mathbf{K} = 0 \quad (\text{dim } \mathbf{I} = n \times n) \tag{13.5}$$

where $\mathbf{I}$ is the identity matrix, yields real eigenvalues ω_i (angular frequencies),
each associated to real eigenvectors $\boldsymbol{\varphi}_i$, that can be ordered in the columns of a
matrix $\boldsymbol{\Phi}$:

$$\boldsymbol{\Phi} = \begin{bmatrix} \varphi_1 & \vdots & \varphi_2 & \vdots & \dots & \vdots & \varphi_n \end{bmatrix} \tag{13.6}$$

The linear system of n time-invariant differential equations of the second order
(Eq. 13.4) can be also written as a set of $2n$ linear time-invariant first order
differential equations in the state-space representation:

$$\dot{\mathbf{z}} = \mathbf{A}\,\mathbf{z} + \mathbf{B}\,\mathbf{f}_d \tag{13.7}$$

where

$$
\begin{aligned}
\mathbf{A} &= \begin{bmatrix} \mathbf{0}_{n \times n} & \mathbf{I}_{n \times n} \\ -\mathbf{M}^{-1}\mathbf{K} & -\mathbf{M}^{-1}\mathbf{C} \end{bmatrix} \quad (\text{dim } \mathbf{A} = 2n \times 2n) \\[2mm]
\mathbf{B} &= \begin{bmatrix} \mathbf{0}_{n \times 1} \\ -\mathbf{M}^{-1}\mathbf{P} \end{bmatrix} \quad (\text{dim } \mathbf{B} = 2n \times m)
\end{aligned}
\tag{13.8}
$$

and

$$\mathbf{z} = [\boldsymbol{\delta}\,\dot{\boldsymbol{\delta}}]^{\mathrm{T}} = \begin{bmatrix} \delta_0 & \dots & \delta_r & \dot{\delta}_0 & \dots & \dot{\delta}_r \end{bmatrix}^{\mathrm{T}} \tag{13.9}$$

is the system state. The $2n$ eigenvalues and eigenvectors of $\mathbf{A}$ fully describe the free motion of the system shown in Fig. 13.13 when uncontrolled ($f_{di} = 0$). In particular, for the structural system considered, the complex eigenvalues s_i come in conjugate pairs which correspond to angular frequencies ω_i and modal damping ratios ξ_i [19] as follows (j is the complex unity):

$$s_{i,ic} = -\zeta_i \omega_i \pm \mathrm{j}\,\omega_i \sqrt{1 - \xi_i^2} \tag{13.10}$$

or, conversely, as

$$\omega_i = |s_i|\;\xi_i = -\frac{\mathrm{Real}(s_i)}{|s_i|}. \tag{13.11}$$

Each modal frequency and damping ratio can be drawn through Eq. 13.11 from either the corresponding eigenvalue s_i or from its complex conjugate $s_{i,c}$. Analogously, the $2n$ eigenvectors of $\mathbf{A}$ come in complex conjugate pairs that can be collected in a $2 \times 2n$ matrix $\boldsymbol{\Psi}$:

$$\boldsymbol{\Psi} = \begin{bmatrix} \boldsymbol{\Psi}_1 & \boldsymbol{\Psi}_{1,c} & \dots & \boldsymbol{\Psi}_n & \boldsymbol{\Psi}_{n,c} \\ s_1\boldsymbol{\Psi}_1 & s_{1,c}\boldsymbol{\Psi}_{1,c} & \dots & s_n\boldsymbol{\Psi}_n & s_{n,c}\boldsymbol{\Psi}_{n,c} \end{bmatrix} \tag{13.12}$$

Each column of the matrix $\boldsymbol{\Psi}$ can be thought as made of 2 n-component vectors. The first n-component vector is actually the complex modal shape, the second part is the modal shape times the corresponding complex frequency. If damping can be neglected, the following equation holds:

$$\boldsymbol{\Phi} = \begin{bmatrix} \varphi_1 & \varphi_2 & \dots & \varphi_n \end{bmatrix} = \begin{bmatrix} \psi_1 & \psi_2 & \dots & \psi_n \end{bmatrix} = \boldsymbol{\Psi}* \tag{13.13}$$

otherwise ψ_i is the complex modal shape corresponding to the real, undamped counterpart φ_i, but explicitly considering the damping. $\boldsymbol{\Psi}*$ here denotes the subset of $\boldsymbol{\Psi}$ directly comparable to $\boldsymbol{\Phi}$.

Let us assume that each control force f_{di}, at a given instant of time, has a specific value f_{ui}, function of the system's state through a gain matrix $\mathbf{G}$ as follows:

$$\mathbf{f}_d(t) = [f_{d1}(t) \quad \dots \quad f_{dm}(t)]^{\mathrm{T}} = \mathbf{f}_u(t) = [f_{u1}(t) \quad \dots \quad f_{um}(t)]^{\mathrm{T}} = -\mathbf{G} \cdot \mathbf{z}(t). \tag{13.14}$$

In this case, the free vibrations (Eq. 13.7) becomes:

$$\dot{\mathbf{z}} = \mathbf{A}\,\mathbf{z} + \mathbf{B}\,\mathbf{f}_d = \mathbf{A}\,\mathbf{z} + \mathbf{B}(-\mathbf{Gz}) = (\mathbf{A} - \mathbf{BG}) = \mathbf{A}_{CL}\,\mathbf{z}. \tag{13.15}$$

Eigenvalues and eigenvectors of $\mathbf{A}_{CL}$ (summarizing the properties of the closed loop controlled system) are different from those of $\mathbf{A}$ or, in other words, frequencies, damping ratios, and modal shapes of the controlled system are different from those of the uncontrolled one. Therefore, a question arises if modal parameters can be modified in a more favorable way. An answer to this question was probably first introduced by Moore [11] and then explored by many scholars, but the authors are unaware of any application to the particular case of SA controlled wind turbines. In the latter case, in order to reduce stresses in the supporting tower, it would be desirable to have a first modal shape of the controlled structure dominated by a highly damped rigid motion around the hinged base and higher modes with mass participation factors close to 0.

Let us assume that a matrix $\mathbf{G}$ does exist so that $s_{d,i}$ and $\boldsymbol{\psi}_{d,i}$ are the desired eigenvalue and eigenvector of the i-th mode of the closed loop (CL) system. When the CL system vibrates according to that mode, the system state varies proportionally to the displacements and velocities described by the corresponding eigenvector:

$$\mathbf{z}(t) = \boldsymbol{\psi}_{d,i} \cdot e^{s_{d,i} \cdot t} \tag{13.16}$$

and in this case the desired control forces $\mathbf{f}_{ui}$ can be expressed as:

$$\mathbf{f}_{ui}(t) = \mathbf{u}_i \cdot e^{s_{d,i} \cdot t} = -\mathbf{G}\,\mathbf{z}(t) = -\mathbf{G}\,\boldsymbol{\psi}_{d,i} \cdot e^{s_{d,i} \cdot t}. \tag{13.17}$$

The product $\mathbf{A}_{CL}.\boldsymbol{\psi}_{d,i}$ can be written as:

$$\mathbf{A}_{CL}\,\boldsymbol{\psi}_{d,i} = (\mathbf{A} - \mathbf{B}\,\mathbf{G})\,\boldsymbol{\psi}_{d,i} = \mathbf{A}\,\boldsymbol{\psi}_{d,i} + \mathbf{B}\left(-\mathbf{G}\,\boldsymbol{\psi}_{d,i}\right) = \mathbf{A}\,\boldsymbol{\psi}_{d,i} + \mathbf{B}\,\mathbf{u}_i. \tag{13.18}$$

Being $s_{d,i}$ and $\boldsymbol{\psi}_{d,i}$ an eigenvalue and the corresponding eigenvector of $\mathbf{A}_{CL}$, the same product is also equal to:

$$\mathbf{A}_{CL}\,\boldsymbol{\psi}_{d,i} = s_{d,i}\,\boldsymbol{\psi}_{d,i}. \tag{13.19}$$

By combining Eqs. 13.18 and 13.19,

$$\mathbf{A}_{CL}\,\boldsymbol{\psi}_{d,i} = \mathbf{A}\,\boldsymbol{\psi}_{d,i} + \mathbf{B}\,\mathbf{u}_i = s_{d,i}\,\boldsymbol{\psi}_{d,i} \tag{13.20}$$

or

$$\mathbf{B}\,\mathbf{u}_i = \left(s_{d,i}\,\mathbf{I} - \mathbf{A}\right)\boldsymbol{\psi}_{d,i} \tag{13.21}$$

and, finally,

$$\boldsymbol{\psi}_{d,i} = \left[\left(s_{d,i}\,\mathbf{I} - \mathbf{A}\right)^{-1}\mathbf{B}\right]\mathbf{u}_i = \mathbf{H}_i\,\mathbf{u}_i \;(\dim \mathbf{H}_i = 2n \times m). \qquad (13.22)$$

Equation 13.22 shows the relationship among the desired eigenvalue $s_{d,i}$ and eigenvector $\boldsymbol{\psi}_{d,i}$, the matrix of the original, uncontrolled system $\mathbf{A}$ and the corresponding control forces $\mathbf{u}_i$, i.e., the control forces able to make the controlled system vibrate according to desired modal shape, frequency and damping ratio. Should the matrix $\mathbf{H}_i$ be invertible, calculation of the control forces $\mathbf{u}_i$ would be straightforward. However, it is generally not. An approximate approach to solve Eq. 13.22 for $\mathbf{u}_i$ is to consider the pseudo-inverse matrix $\mathbf{H}_i^{\wedge}$ of $\mathbf{H}_i$. In this case, $\mathbf{u}_i$ can be approximately evaluated as

$$\mathbf{u}_i = \mathbf{H}_i^{\wedge}\boldsymbol{\psi}_{d,i} = \left[\left(\mathbf{H}_i^{\mathrm{T}}\,\mathbf{H}_i\right)^{-1}\mathbf{H}_i^{\mathrm{T}}\right]\boldsymbol{\psi}_{d,i}. \qquad (13.23)$$

However, by using the approximation expressed by Eq. 13.23, the actual eigenvector $\boldsymbol{\psi}_{\mathrm{CL},i}$ of the CL system will be similar, but not exactly equal to the desired one $\boldsymbol{\psi}_{d,i}$:

$$\boldsymbol{\psi}_{\mathrm{CL},i} = \mathbf{H}_i\,u_i \cong \boldsymbol{\psi}_{d,i}. \qquad (13.24)$$

If the approximation of Eq. 13.23 is acceptable, by selecting the desired frequency and damping ratio (through $s_{d,i}$) and the shape (through $\boldsymbol{\psi}_{\mathrm{CL},i}$) of each mode of vibration, it is possible to calculate the corresponding values of the desired control forces $\mathbf{u}_i$ and the resulting CL eigenvector $\boldsymbol{\psi}_{\mathrm{CL},i}$, to be collected in the matrices $\mathbf{U}$ and $\boldsymbol{\Psi}_{\mathrm{CL}}$, respectively:

$$\begin{aligned} \mathbf{U} &= \begin{bmatrix} u_1 & u_2 & \ldots & u_{2n} \end{bmatrix} \quad (\dim \mathbf{U} = m \times 2n) \\ \boldsymbol{\Psi}_{\mathrm{CL}} &= \begin{bmatrix} \boldsymbol{\psi}_{\mathrm{CL},1} & \boldsymbol{\psi}_{\mathrm{CL},2} & \cdots & \boldsymbol{\psi}_{\mathrm{CL},2n} \end{bmatrix} \quad (\dim \boldsymbol{\Psi}_{\mathrm{CL}} = 2n \times 2n). \end{aligned} \qquad (13.25)$$

Recalling Eq. 13.17, it is:

$$\mathbf{U} = -\mathbf{G}\,\boldsymbol{\Psi}_{CL} \qquad (26)$$

and, therefore, the gain matrix can be found as

$$\mathbf{G} = -\,\mathbf{U} \cdot \boldsymbol{\Psi}_{\mathrm{CL}}^{-1}. \qquad (13.27)$$

Once $\mathbf{G}$ is calculated through Eq. 13.27, the corresponding control forces $\mathbf{f}_u$ defined by Eq. 13.14 are able to approximately transform the original structure so that it has the desired modal properties:

- frequency and damping ratio of each selected mode;
- modal shapes.

It is worth to notice that the procedure described before works also if only a portion of a CL eigenvector is desired to have a given shape. In other words, the selection can be also referred to portions of some or all CL eigenvectors. Due to the approximate calculations introduced before, the less demanding is the eigenvector selection, the most accurate is the result, i.e., the closer are CL and desired eigenvectors.

Provided that more than one independent controller be available and that the positioning of such controllers yields a controllable system, for a feed-back controlled wind turbine it is thus possible to directly design the modal behavior, in terms of both modal frequencies and damping ratio, and modal shapes. When there is only one controller available, as in the case of the experimental activity described herein, it is possible to directly design modal frequencies and damping ratio only, and to indirectly control modal shapes.

13.5.1 Closed-Loop Eigenstructure Selection (CLES) Algorithm

A simplified structural model of the wind turbine mock up described in the previous sections is shown in Fig. 13.14. It is a 2 DOFs system whose equations of motion in the absence of any external disturbance are:

$$
\begin{bmatrix} m_T & m_T \\ 0 & m_\alpha/h \end{bmatrix} \begin{bmatrix} \ddot{\delta}_{el} \\ \ddot{\delta}_{rig} \end{bmatrix} + \begin{bmatrix} c_T & 0 \\ 0 & 0 \end{bmatrix} \begin{bmatrix} \dot{\delta}_{el} \\ \dot{\delta}_{rig} \end{bmatrix} + \begin{bmatrix} k_T & 0 \\ 0 & 2 \cdot k_s \cdot l_s^2/h \end{bmatrix} \begin{bmatrix} \delta_{el} \\ \delta_{rig} \end{bmatrix}
$$
$$
= - \begin{bmatrix} 0 \\ 2 \cdot l_d \end{bmatrix} \cdot f_d \tag{13.28}
$$

or

$$
\mathbf{M}\ddot{\delta} + \mathbf{C}\dot{\delta} + \mathbf{K}\delta = -\mathbf{p}f_d \tag{13.29}
$$

where:

$m_T = m_{top} + m_{tow}$	is the translational mass of the model;
$m_{top} = 280$ kg	is the translational mass at the top of the tower;
$m_{tow} = 15.4$ kg	is the 1st mode translational mass of the vertical structure;
$m_\alpha = 8{,}329$ kg m^2	is the rotational mass of the model;
$c_T = 32.4$ Ns/m	is the equivalent linear viscous damping of the tower;
$k_T = 13{,}855$ N/m	is the lateral stiffness of the tower;
$k_s = 89{,}000$ N/m	is the stiffness of each base spring;
$l_s = 0.65$ m	is distance between each spring and the hinge;
$l_d = 0.45$ m	is distance between each SA MR damper and the hinge;
$h = 5.26$ m	is the height of the tower;
f_d	is the force exerted by each SA MR damper;
α	is the rotation of the base;
$\delta_{rig} = \alpha \times h$	is the rigid portion of the top displacement;

Fig. 13.14 Structural model
of the tested mock-up
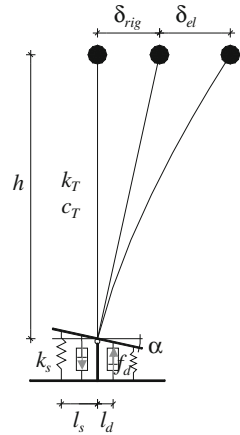
δ_{el} is the elastic part of the top displacement;
M, C, and **K**   are the mass, damping, and stiffness matrices;
p   is the vector describing the position of the dampers;
$\delta = [\delta_{el}\ \delta_{rig}]^T$ is the vector collecting the DOFs of the system.

Parameters c_T and k_T have been defined according to a preliminary identifi-
cation campaign of the fixed base tower, which turned out to show a natural period
of vibration of 0.92 s and a damping ratio equal to 0.8 % [12, 13]. Once the tower
is mounted on the rotating support, the resulting 2 DOFs free ($f_d = 0$) system
described by Eq. 13.28 has modal periods equal to:

$$\text{1st mode}: \quad T_1 = 2.09\,\text{s};$$
$$\text{2nd mode}: \quad T_2 = 0.92\,\text{s}.$$

The first mode is dominated by a rigid rotation around the base hinge, whereas the
second replies the elastic motion of the tower alone on a fixed base, as shown in
Eq. 13.30 where the undamped modal shapes are ordered as columns of the matrix $\mathbf{\Phi}$
and normalized, for clarity, so that one component of each eigenvector is set to 1:

$$\mathbf{\Phi} = \begin{bmatrix} 1.000 & 0.000 \\ 0.239 & 1.000 \end{bmatrix} \begin{pmatrix} \delta_{\text{rig}} \\ \delta_{\text{el}} \end{pmatrix}. \tag{13.30}$$

By considering the dampers in their "off" state, they are equivalent to linear
viscous damper with a constant $c_d = 6{,}900$ Ns/m [17]. In this case, the force in
each damper is equal to (the sign is already considered in the model of Fig. 13.14).

$$f_d = c_d \cdot l_d \cdot \dot{\delta}_{\text{rig}}/h \tag{13.31}$$

and Eq. 13.28 can be written as

$$\begin{bmatrix} m_T & m_T \\ 0 & m_\alpha/h \end{bmatrix} \begin{bmatrix} \ddot{\delta}_{el} \\ \ddot{\delta}_{rig} \end{bmatrix} + \begin{bmatrix} c_T & 0 \\ 0 & 2 \cdot c_d \cdot l_d^2/h \end{bmatrix} \begin{bmatrix} \dot{\delta}_{el} \\ \dot{\delta}_{rig} \end{bmatrix} + \begin{bmatrix} k_T & 0 \\ 0 & 2 \cdot k_s \cdot l_s^2/h \end{bmatrix} \begin{bmatrix} \delta_{el} \\ \delta_{rig} \end{bmatrix} = \begin{bmatrix} 0 \\ 0 \end{bmatrix}.$$

(13.32)

or

$$\mathbf{M}\ddot{\boldsymbol{\delta}} + \mathbf{C}_{off}\,\dot{\boldsymbol{\delta}} + \mathbf{K}\,\boldsymbol{\delta} = \mathbf{0} \qquad (13.33)$$

being $\mathbf{C}_{off}$ the damping matrix when the SA MR dampers are switched off. This system can be equivalently described in the state space as

$$\dot{\mathbf{z}} = \mathbf{A}_{off}\,\mathbf{z} \qquad (13.34)$$

where $\mathbf{z}$ is the state vector of the system and $\mathbf{A}_{off}$ is the matrix describing the dynamic behavior of the tested model when the dampers are switched off, defined as follows:

$$\mathbf{z} = \begin{bmatrix} \delta_{el} & \delta_{rig} & \dot{\delta}_{el} & \dot{\delta}_{rig} \end{bmatrix}^T; \quad \mathbf{A}_{off} = \begin{bmatrix} \mathbf{0}_{2\times2} & \mathbf{I}_{2\times2} \\ -\mathbf{M}^{-1}\mathbf{K} & -\mathbf{M}^{-1}\mathbf{C}_{off} \end{bmatrix} \qquad (13.35)$$

The complex eigenvalues of $\mathbf{A}_{off}$ describe the periods T_i and the modal damping ratios ξ_i of the tested model. They are as follows:

$$1\text{st mode}: \quad T_1 = 2.09\,\text{s} \quad \xi_1 = 5.6\,\%;$$
$$2\text{nd mode}: \quad T_2 = 0.92\,\text{s} \quad \xi_2 = 0.8\,\%.$$

The first objective of the control algorithm is to achieve higher damping ratios without changing the periods of vibration. This objective can be reached through the classical pole placement procedure of System's Theory. If a "desired" force u for each damper is assumed, Eq. 13.29 can be written, in the state space, as

$$\dot{\mathbf{z}} = \mathbf{A}\,\mathbf{z} + \mathbf{b}\,u \qquad (13.36)$$

where

$$\mathbf{A} = \begin{bmatrix} \mathbf{0}_{2\times2} & \mathbf{I}_{2\times2} \\ -\mathbf{M}^{-1}\mathbf{K} & -\mathbf{M}^{-1}\mathbf{C} \end{bmatrix} \quad \mathbf{b} = \begin{bmatrix} \mathbf{0}_{2\times1} \\ -\mathbf{M}^{-1}\mathbf{p} \end{bmatrix} \qquad (13.37)$$

If the control force is proportional to the system's state through Eq. 13.14, it can be showed that the gain matrix $\mathbf{G}$ can be designed so as that the eigenvalues of the controlled system can be arbitrarily assigned or, in other words, the desired

values of damping ratios and natural periods can be achieved [10]. Therefore, the matrix **G** can be designed so as to achieve the first objective of maintaining the modal periods while increasing the modal damping ratios.

As said before, within the experimental setup herein focused, only one independent control force was available, provided by the 2 SA MR dampers. Should more independent control forces be available, the gain matrix **G** could be designed to arbitrarily modify the modal shapes of the controlled system, too. Actually, this is the second objective of the control strategy adopted, i.e., to modify the modal behavior of the tower so as to obtain a dominant, highly damped mode corresponding to a rigid rotation of the structure around the base hinge and a secondary mode combining a rigid rotation to an elastic deformation of the tower bounded by a damping ratio significantly higher than that of the tower alone (0.8 %). Due to the presence of only one independent controller, the procedure described before cannot be applied. However, also the pole placement technique modifies, through **G**, the CL system matrix and, in turn, its complex eigenvectors (i.e., the modal shapes of the controlled tower). Therefore, when the desired control force u is designed through Eq. 13.14 so as to obtain the given values of periods of vibration and modal damping ratios for the CL system, also the modal shapes of the controlled system change compared to the original, uncontrolled one. Based on a trial and error iterative procedure, authors ended up with the following feedback control law:

$$u = -2 \cdot \begin{bmatrix} g_1 & g_2 & g_3 & g_4 \end{bmatrix} \cdot \mathbf{z} \qquad (13.38)$$

where:

$g_1 = 597$ N/m; $g_2 = 0$; $g_3 = 408$ Ns/m; $g_4 = 1{,}154$ Ns/m.

In this case, the CL controlled tower shows the following periods and damping ratios:

$$\text{1st mode}: \quad T_1 = 2.09\,\text{s} \quad \xi_1 = 20\,\%;$$
$$\text{2nd mode}: \quad T_2 = 0.92\,\text{s} \quad \xi_2 = 5\,\%.$$

Correspondingly, the complex eigenvectors of the controlled towers, ordered as columns of the matrix $\mathbf{\Psi}^*$ and normalized as before, are:

$$\mathbf{\Psi}_* = \begin{bmatrix} |1.000| \angle 0° & |0.084| \angle 93° \\ |0.234| \angle -27° & |1.000| \angle 0° \end{bmatrix} \begin{pmatrix} \delta_{\text{rig}} \\ \delta_{\text{el}} \end{pmatrix} \qquad (13.39)$$

Equation 13.39 shows only a portion ($\mathbf{\Psi}^*$) of the eigenvector matrix $\mathbf{\Psi}$ of the controlled tower. Indeed, in the present case the eigenvectors come in complex conjugate pairs carrying, each pair, exactly the same piece of information. Furthermore, each eigenvector has four components, two related to displacements (shown in Eq. 13.39) and two relates to velocities (out of interest in the present case). Complex eigenvectors in Eq. 13.39 are described through their module and

phase. The first mode resulted to be dominated by a rigid rotation of the tower around the base with a reasonably high damping ratio, whereas the second mode is dominated by the elastic strain of the tower. For the latter, however, in the controlled system a rigid rotation is also involved, so that a damping ratio of about 5 % ($\gg$0.8 %) can be obtained due to the SA MR dampers.

If active devices had been involved, the force $u(t)$ should be imposed instant by instant to them in order to achieve the target performances of the structure. In the present case of SA control, instead, this force has to be intended as a desired control action, that is the one the MR dampers have to mimic in real time to lead to an effective control of the tower response. Therefore, the CLES algorithm has been set so as to modulate the current fed to the SA MR dampers with the aim to make the reacting force $f_d(t)$ of each damper as close as possible to the theoretical value $u(t)$. This kind of logic can thus be expressed as follows:

$$
\begin{array}{llll}
\text{if} & f_d(t) \cdot u(t) < 0 & \rightarrow & i(t) = 0 \\
\text{if} & f_d(t) \cdot u(t) \geq 0 \quad \text{and} \quad |f_d(t)| < |u(t)| & \rightarrow & i(t) = i(t - \mathrm{d}t) + [i_{\max} - i(t - \mathrm{d}t)/n] \\
\text{if} & f_d(t) \cdot u(t) \geq 0 \quad \text{and} \quad |f_d(t)| \geq |u(t)| & \rightarrow & i(t) = i(t - \mathrm{d}t) + [0 - i(t - \mathrm{d}t)/n]
\end{array}
\tag{13.40}
$$

where $i(t$–$\mathrm{d}t)$ is the current commanded to the dampers in the instant before the actual one (t), $\mathrm{d}t$ is the sampling time for control (1 ms), n is a dimensionless parameter (≥ 1) introduced to smoothen the variation of the command current between 0 and $i_{\max}$.

13.5.2 Two Variables (2VAR) Algorithm

An alternative control algorithm has been formulated and adopted for the shaking table tests of the wind turbine model. It is based on a more physical and easier approach in respect to the above-mentioned CLES controller.

The basic idea consists in controlling the base stress and top displacement so as to "force" them to be within a given range. Reducing top displacement and base stress are two performance objectives in conflict to each other. Actually, the demand of base bending stress can be reduced by "relaxing" the base restraint (i.e., reducing the damping of the SA devices). However, as a direct consequence, the top displacement demand (related to both the rigid body motion—due to the base rotation—and the elastic deflection of the tower) will increase.

This controller has been developed aiming to achieve a trade-off between these two contradictory objectives. To do that, first of all, a limit value for both base stress and top displacement have been assumed (σ_{lim} and x_{lim} in the following, respectively). Then, by denoting with $\sigma(t)$, $x(t)$ and $\dot{x}(t)$, respectively, the maximum stress at the base, the top displacement, and the top velocity at the instant of

time t, the following logic has been assumed to take the decision about the optimal status ("on" or "off") to be set for the dampers in that instant:

$$\text{if} |\sigma(t)| < \sigma_{\text{lim}} \quad \rightarrow i(t) = i_{\text{max}} \tag{13.41}$$

$$\text{if} |\sigma(t)| \geq \sigma_{\text{lim}} \text{ and } |x(t)| < x_{\text{lim}} \quad \rightarrow i(t) = 0 \tag{13.42}$$

$$\text{if } |\sigma(t)| \geq \sigma_{\text{lim}} \text{ and } |x(t)| \geq x_{\text{lim}} \text{and } x(t)\dot{X}(t) > 0 \rightarrow i(t) = i_{\text{max}} \tag{13.43}$$

$$\text{if } |\sigma(t)| \geq \sigma_{\text{lim}} \text{ and } |x(t)| \geq x_{\text{lim}} \text{ and } x(t)\dot{X}(t) \leq 0 \rightarrow i(t) = 0. \tag{13.44}$$

In other words, the controller keeps "stiffer" the base restraint until the stress does not exceed the limit value (Eq. 13.41), whereas "relaxes" it (switching off the MR dampers) when this limit is passed and the displacement falls within the limits (Eq. 13.42). When both stress and displacement are beyond the respective threshold values, the controller switches on the dampers if the displacement is going in the direction of a further increase (so trying to invert or at least to damp this trend; Eq. 13.43), otherwise it switches off the MR devices to make sure they do not hinder the ongoing reduction of displacement (Eq. 13.44).

Figure 13.15 graphically describes this algorithm, in a schematic way, showing what is the decision of the controller (switch on or switch off) depending on the occurrence of each of the four above-mentioned possible combination about the state of base stress and top displacement.

It is worth noting that the practical use of such control algorithm require a preliminary calibration through properly setting the three involved parameters, i.e. i_{max}, σ_{lim} and x_{lim}.

13.6 Experimental Activity and Results

Two load cases were considered:

- an extreme operating gust (EOG), i.e., a sharp increase, then decrease in wind speed within a short period of time;
- a high velocity wind buffeting, i.e., a load case (called "parking", PRK) that typically concerns a wind turbine when "parked" (with a controlled shutdown) due to the high-velocity wind.

Chen and Georgakis [12, 13], for both load cases, have defined an equivalent base acceleration time history (Fig. 13.16), that is the base input that would give the same top mass response of the real, fixed base structure subjected to the wind action. This kind of analysis has been made using the wind turbine aeroelastic code HAWC2 (Horizontal Axis Wind turbine simulation Code, second generation), realized at the DTU (Denmark) for calculating wind turbine response in time

Fig. 13.15 The logic behind the 2VAR controller (numbers refer to Eqs. 13.41–13.44)
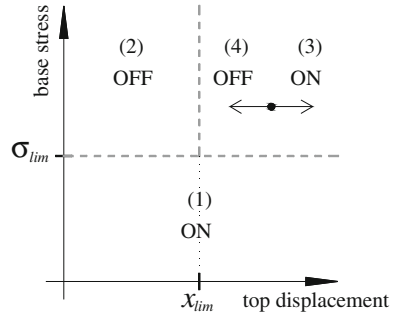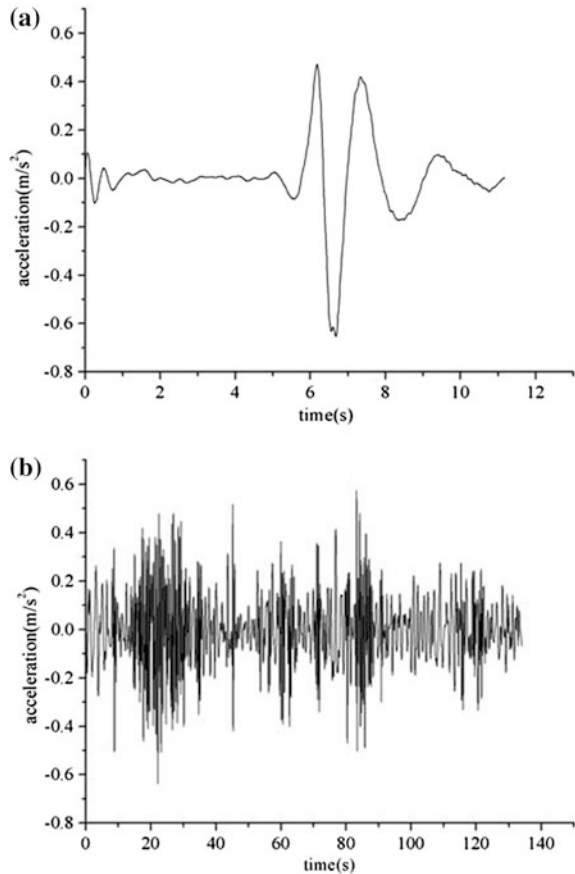

Fig. 13.16 Equivalent base accelerations corresponding to the two wind load cases: **a** Extreme operating gust (EOG), **b** Parking (PRK)

domain [20]. These accelerograms have been reproduced through the shaking table facility to perform all the dynamic tests discussed in the following.

The mock-up structure has been tested first in a fixed base (FB) condition. The FB configuration has been realized using the same setup of Fig. 13.4, simply

Table 13.1 Fixed base con-
dition: peak response of the
tower under both load cases

input	max$|\sigma|$ [MPa]	max$|x|$ [mm]
EOG	51	39
PRK	29	25

imposing the MR dampers to work as rigid links, feeding them with a constant
current of 3 A during the overall duration of the tests. Actually the expected (then
registered) maximum force applied to the dampers for the two FB tests were less
than 5 kN, therefore much less than the threshold value for the "friction" force F_{dy}
of the devices (about 27 kN for 3 A, according to Eq. 13.3). Table 13.1 summa-
rizes the peak absolute value for displacement x (top of the tower relative to the
base) and for base stress σ for both load cases.

The structural model has been tested first using the CLES control algorithm.
The higher value of the dimensionless parameter n involved in the procedure, as
previously said, gives smoother variations of command voltage in time. According
to the results of three pre-tests, the values $n = 15$ for the EOG load case and $n = 1$
for PRK load case were selected.

Subsequently, various tests have been performed with the 2VAR control
algorithm to evaluate and compare the effects, in terms of reduction of the
structural response, of different couples of stress (σ_{lim}) and displacement (x_{lim})
limits chosen within the ranges [10, 40] MPa and [16, 46] mm respectively. The
best combination of limit values resulted to be (σ_{lim}, x_{lim}) = (30 MPa, 46 mm) for
the EOG load case, and (σ_{lim}, x_{lim}) = (12 MPa, 20 mm) for the PRK input.

For each of the above-mentioned tests the reduction of the base stress has been
monitored as the first objective to be achieved. Moreover, the effectiveness in
controlling top displacement has been evaluated, even if a moderate increase has
been considered acceptable. In particular, peak top displacement less than 1.3
times the peak registered in the FB condition have been tolerated, not causing
significant detrimental second order effects to the tower.

The main experimental results related to the four tests (two load cases, two
controllers) are described in the next sections, first with reference to the EOG, then
to the PRK load cases.

In the following, the command voltage has to be intended as a 0–10 V voltage
signal in output from the controller (PC) and in input to the power supplies, the
latter having, when adopted as current driver, a control loop gain 0.4 A/V. The
maximum intensity of current inside the dampers for all the tests has been set equal
to 1 A. Therefore, the maximum command signal is 2.5 V.

13.6.1 SA Control for the Extreme Operating Gust Load Case

An extreme operating gust (EOG) is a sharp increase and then decrease in wind speed that occurs over a short period of time while the turbine is operating. The equivalent base acceleration time history in Fig. 13.16 has been considered herein to assess the effectiveness of both SA control strategies, reproducing such input signal through the DTU shaking table, properly commanding the MTS actuator.

In the following, the results obtained with the CLES controller are described first, then those corresponding to the 2VAR logic.

13.6.1.1 CLES Controller: Response Reduction Under the EOG Load Case

The desired control force $u(t)$ as defined in Sect. 13.5.1 has been calculated in real time during the entire duration of the test. The CLES controller modulated the command signal so as to make the current vary between 0 and 1 A, aiming, at each instant of time, at making the MR reactive force as close to $u(t)$ as possible.

Figure 13.17 shows the results in terms of base stress, top displacement, command voltage, and forces, desired and actual force exerted by MR dampers, respectively. The time window 4–10 s has been plotted, i.e., that corresponding to the most significant part of the accelerogram imposed at the base. The first two diagrams—(a) and (b)—allow to compare the SA controlled response to that corresponding to the FB condition, under the same input base motion.

The actual control force of the MR dampers satisfactory tracked the desired one (Fig. 13.17d), thanks to the modulation of the command voltage according to the above-mentioned logic (Fig. 13.17c). This lead, as expected, to a strong reduction of base stress, trading off larger peak top displacement, however, within the tolerance assumed in respect to the one registered for the FB case. Table 13.2 helps synthesize such findings, in terms of peak values of base stress and of top displacement recorded for the whole duration of the test. The CLES controller, in respect to the FB case, reduced the peak base stress of 67 %, even at the cost of 28 % larger peak top displacement.

13.6.1.2 2VAR Controller: Response Reduction Under the EOG Load Case

The performance of the 2VAR controller with limit values of σ_{lim} and x_{lim} equal to 30 MPa and 46 mm, respectively, is described in the following. Figure 13.18 shows the results in terms of base stress, top displacements, and command voltage, allowing the comparison with the FB response under the same base input motion. The first two diagrams—(a) and (b)—are referred to the overall duration of the
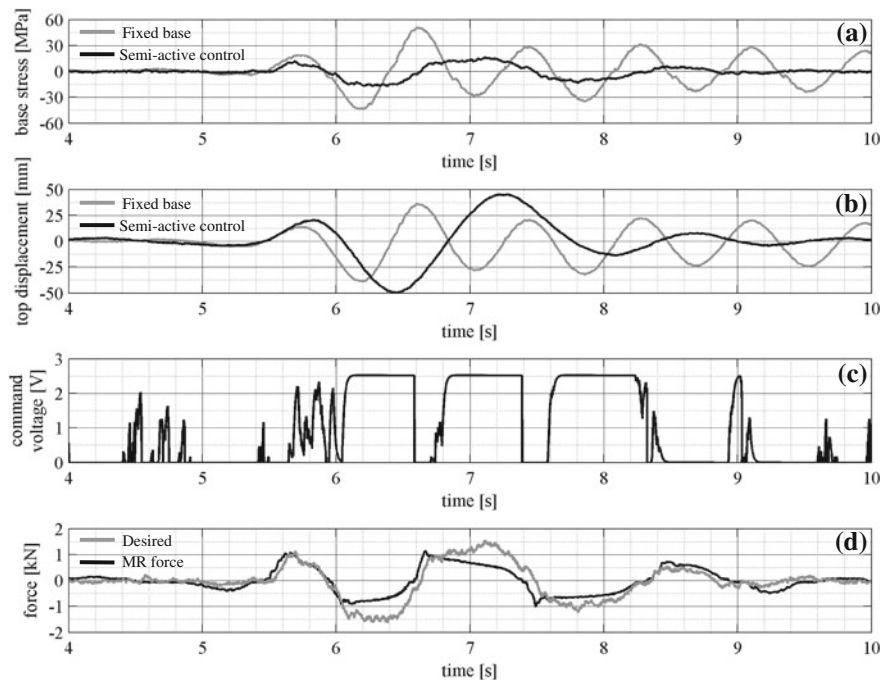
Fig. 13.17 EOG load case: SA control via the CLES controller and comparison with the FB case

Table 13.2 EOG input: peak response of the FB structure and of the SA case using the CLES controller

Case	max|σ|	max|x|
Fixed base	51 MPa	39 mm
Semi-active CLES	17 MPa	50 mm
FB → SA	−67 %	+28 %

Percentage variation from the first to the second condition

EOG accelerogram, whereas diagrams (c), (d), and (e) are focused on a 2 s time window (5.5–7.5 s), so highlighting the behavior of the uncontrolled and controlled tower during the strongest phase of the base excitation.

It can be observed that the top displacement always resulted to be within the limit of 46 mm, therefore only conditions in Eqs. 13.41 and 13.42 occurred. Figure 13.18c–e highlights the position of two instants of time (6.19 and 6.77 s) where the condition of Eq. 13.42 and of Eq. 13.41, respectively occurred, causing a switch-off and a switch-on of the current in the devices. Looking again at Fig. 13.18, the reduction of stress and displacement compared to FB case (except for the peak displacement) is quite evident. In particular, around the strong phase of the excitation, the control algorithm, also thanks the promptness of the control
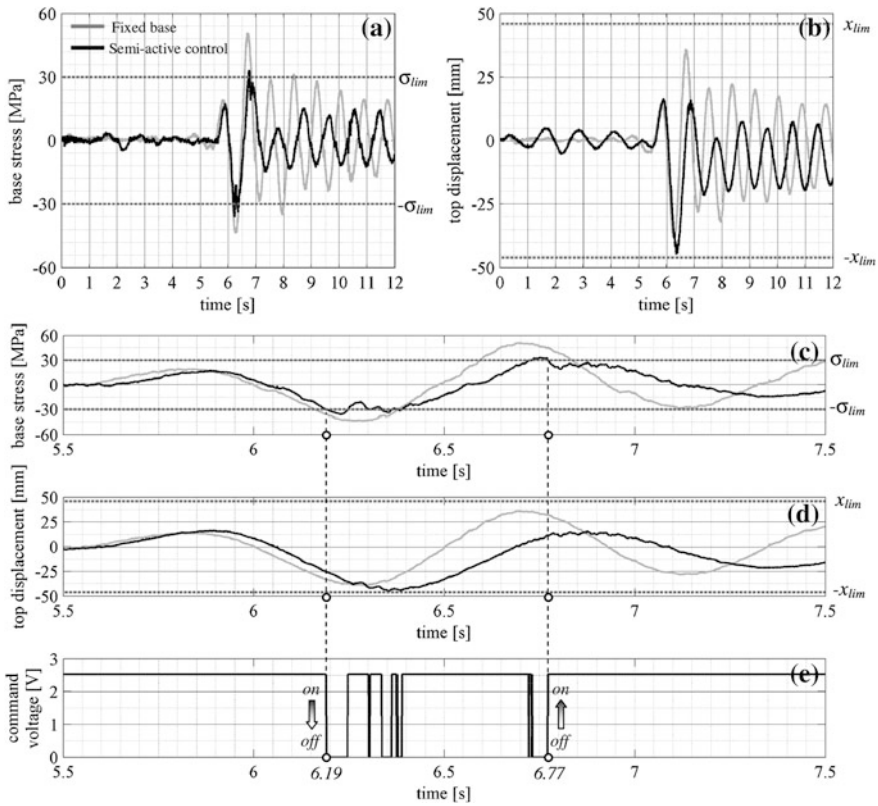
Fig. 13.18 EOG load case: SA control via the 2VAR controller and comparison of the response with the FB case

chain, perfectly worked in "pushing down" the peak values of stress demand, forcing it to stay within the fixed limits.

Table 13.3, as for the CLES controller examined above, shows the peak values of base stress and top displacement for the FB and the 2VAR controlled cases. It allows to conclude that the 2VAR control logic, in respect to the FB case, reduced the peak base stress of 29 %, even at the cost of a 15 % increase of the peak top displacement.

13.6.2 SA Control for the Parking Load Case

When a pitch-controlled wind turbine shuts down due to the high-velocity wind, the loss of power leads to a sudden pitch of the rotor blades, leading to a "sling-shot" effect, followed by a free-decay response. When parked, the wind turbine

Table 13.3 EOG input: peak response of the FB structure and of the SA case using the 2VAR controller

Case	max|σ|	max|x|
Fixed base	51 MPa	39 mm
Semi-active 2VAR	36 MPa	45 mm
FB → SA	−29 %	+15 %

Percentage variation from the first to the second condition

will be subjected to high velocity wind buffeting, which is herein referred to as "parking" (PRK) load case.

The equivalent base acceleration time history in Fig. 13.16 has been considered to assess the effectiveness of both SA control strategies, reproducing such input signal by the shaking table. In the following, the results obtained with the CLES controller first, then with the 2VAR control logic, are discussed. Since the long duration of the input (more than 2 min), a 10 s time window has been chosen to plot the response time-histories, not to lose their readability and to show in a clearer manner how the controllers worked.

For the PRK load case, the control activity resulted to be higher than in the EOG case. The control algorithms switched on or off the MR devices many more times, making them able to better dissipate the input energy. From this perspective, the higher acceleration demand (value and number of peaks) corresponding to the PRK load case justifies the better response reduction achieved by the same SA system if compared to the EOG input.

13.6.2.1 CLES Controller: Response Reduction Under the PRK Load Case

Figure 13.19 shows the results in terms of base stress, top displacements, command voltage, and forces, respectively desired and actually exerted by MR dampers, within the selected 10 s time window. Also in this case, the controller has been able to drive MR dampers to react similarly to the ideal device, i.e., the one that would exactly output the desired control force $u(t)$. With reference to the assumed sample time window, Fig. 13.19 clearly shows that the CLES controller lead to a strong reduction of the base stress, without significantly altering the response in terms of displacement. Confirming this finding, Table 13.4 shows peak values, over the entire input duration, of base stress and top displacement and their percentage variation in respect to the FB case. The peak base stress results to be reduced of 48 %, while the peak top displacement did not change appreciably.
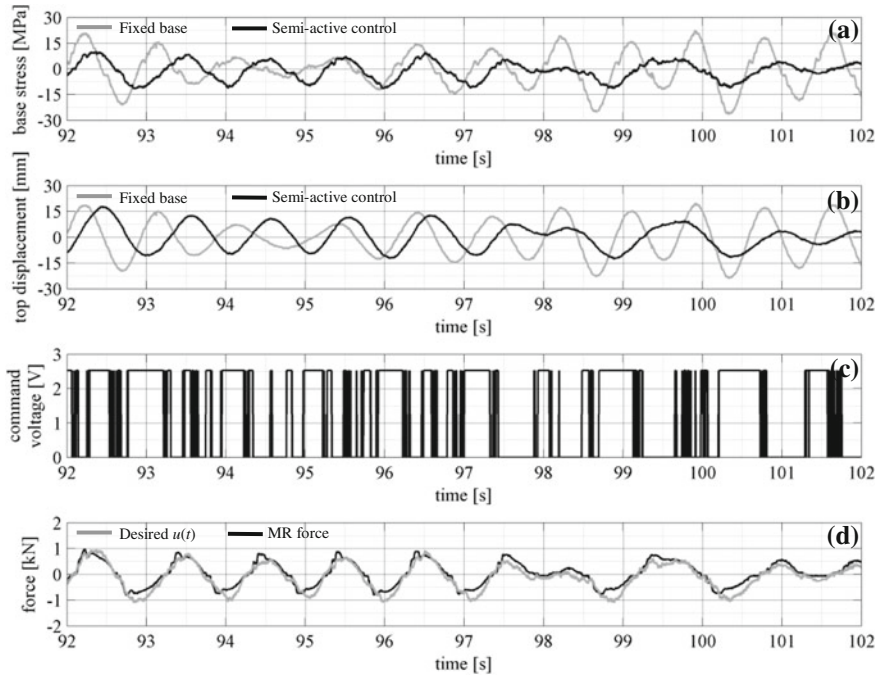
Fig. 13.19 PRK load case: SA control via the CLES controller and comparison of the response with the FB case

Table 13.4 PRK input: peak response of the FB structure and of the SA case using the CLES controller

Case	max|σ|	max|x|
Fixed base	29 MPa	25 mm
Semi-active CLES	15 MPa	25 mm
FB → SA	−48 %	0 %

Percentage variation from the first to the second condition

13.6.2.2 2VAR Controller: Response Reduction Under the PRK Load Case

The 2VAR controller for the PRK input has been set with $\sigma_{lim} = 12$ MPa and $x_{lim} = 20$ mm, as said above. Figure 13.20 shows the results in terms of base stress, top displacements, and command voltage, allowing the comparison with the FB response under the same base input motion, over the above 10 s time window.

The effectiveness of the SA control strategy based on the 2VAR logic clearly emerges comparing the plots of the response parameters with those referred to the FB case. As a matter of a fact, both base stress and top displacement in the SA test result to be forced by the controller to stay within the assigned limits.
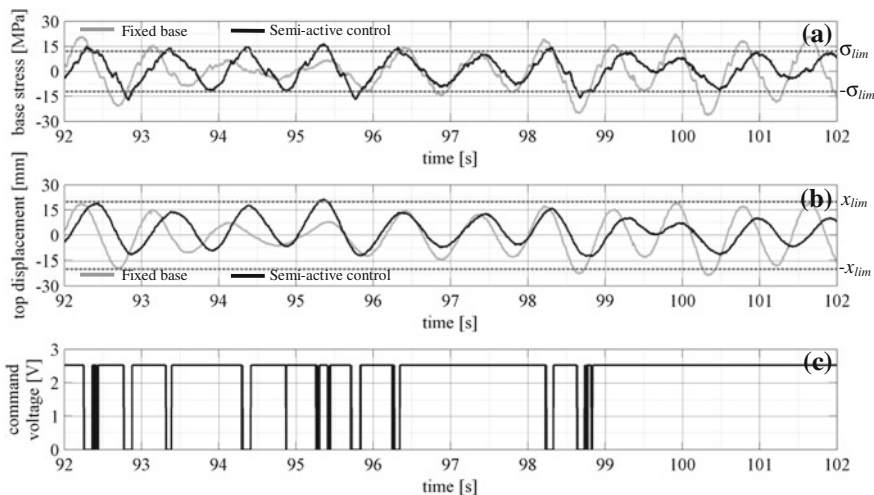
Fig. 13.20 PRK load case: SA control via the 2VAR controller and comparison of the response with the FB case

Table 13.5 PRK input: peak response of the FB structure and of the SA case using the 2VAR controller

Case	max|σ|	max|x|
Fixed base	29 MPa	25 mm
Semi-active 2VAR	20 MPa	23 mm
FB → SA	–31 %	–8 %

Percentage variation from the first to the second condition

As previously done with reference to the other application, the peak values for base stress and top displacement are assumed as synthetic indicators of the response for both FB and 2VAR controlled cases. Table 13.5 shows these values and the percentage variation from the FB to the SA case. It allows to conclude that the 2VAR control logic, for the PRK load case, lead to a significant reduction of the peak base stress (31 %), even if smaller than the one (48 %) obtained with the CLES controller. On the other hand, the 2VAR control logic has also been able to damp the top displacement, making the peak value 8 % smaller with respect to the FB case.

13.7 Conclusions

The theoretical base and the experimental activity about an SA control system for wind turbines based on MR devices has been described. The main findings of the research activity are as follows:

- Structural control of wind turbines based on SA MR dampers and on a base restraint rearrangement of the tower looks feasible;
- Significant reduction of stresses in the turbine tower can be reached trading off a minor increase of the top displacement. Due to the proposed control system, however, displacements of the tower are only partly related to strain;
- Obviously, control algorithms play a relevant role in the behavior of the controlled systems. However, in judging their performances the complexity and the overall reliability of the system (number and type of sensors, real-time computing effort needed) should be taken into account.

A further optimization of the response of a wind turbine can be envisioned by considering the possibility of fully reshaping the modal behavior. The theoretical base of such a strategy is also presented herein, based on the exploitation of more than one independent control force. The possibility of adopting multiple SA MR dampers in the structural control of wind turbines represents the next research step, currently in progress, of the research activity.

References

1. Kirkegaard PH, Nielsen SRK, Poulsen BL, Andersen J, Pedersen LH, Pedersen BJ (2002) Semiactive vibration control of wind turbine tower using an MR damper, structural dynamics: EURODYN 2002. Balkema Publishers A.A., Taylor and Francis, Netherlands, Rotterdam, pp 1575–1580
2. Karimi HR, Zapateiro M, Luo N (2010) Semiactive vibration control of offshore wind turbine towers with tuned liquid column dampers using h_∞ output feedback control. In: Proceedings of IEEE international conference on control applications, Yokohama, Japan
3. Luo N, Bottasso CL, Karimi HR, Zapateiro M (2011) Semiactive control for floating offshore wind turbines subject to aero-hydro dynamic loads. In: Proceedings of international conference on renewable energies and power quality—ICREPQ 2011, Las Palmas de Gran Canaria, Spain
4. Luo N (2011) Smart structural control strategies for the dynamic load mitigation in floating offshore wind turbines. In: Proceedings of international workshop on advanced smart materials and smart structures technology—ANCRiSST, Dalian, China
5. Luo N (2012) Analysis of offshore support structure dynamics and vibration control of floating wind turbines. USTC J 42(5):1–8
6. Luo N, Pacheco L, Vidal Y, Li H (2012) Smart structural control strategies for offshore wind power generation with floating wind turbines. In: Proceedings of international conference on renewable energies and power quality—ICREPQ 2012, Santiago de Compostela, Spain
7. Luo N, Pacheco L, Vidal Y, Zapateiro M (2012) Dynamic load mitigation for floating offshore wind turbines supported by structures with mooring lines. In: Proceedings of european conference on structural control—EACS, Genova, Italy
8. Arrigan J, Pakrashi V, Basu B, Nagarajaiah S (2011) Control of flapwise vibrations in wind turbine blades using semi-active tuned mass dampers. Struct Control Health Monit 18:840–851. doi:10.1002/stc.404
9. Rodríguez TA, Carcangiu CE, Amo I, Martin M, Fischer T, Kuhnle B, Scheu M (2011) Wind turbine tower load reduction using passive and semi-active dampers. In: Proceedings of the european wind energy conference—EWEC 2011, Brussels, Belgium
10. Luenberger DG (1979) Introduction to dynamic systems. John Wiley and Sons, New York

11. Moore BC (1976) On the flexibility offered by state feedback in multivariable systems beyond closed loop eigenvalue assignment. IEEE Trans Autom Control 21:689–692
12. Chen J, Georgakis CT (2013) Tuned rolling-ball dampers for vibration control in wind turbines. J Sound Vib 332:5271–5282. doi:10.1016/j.jsv.2013.05.019
13. Chen J, Georgakis CT (2013) Spherical tuned liquid damper for vibration control in wind turbines. J Vib Control, SAGE Pbs, (in press). doi:10.1177/1077546313495911
14. Caterino N, Spizzuoco M, Occhiuzzi A (2011) Understanding and modeling the physical behavior of magnetorheological dampers for seismic structural control. Smart Mater Struct 20:065013. doi:10.1088/0964-1726/20/6/065013
15. Occhiuzzi A, Spizzuoco M, Serino G (2003) Experimental analysis of magnetorheological dampers for structural control. Smart Mater Struct 12:703–711. doi:10.1088/0964-1726/12/5/306
16. Carlson JD, Jolly MR (2000) MR fluid, foam and elastomer devices. Mechatronics 10:555–569
17. Caterino N, Spizzuoco M, Occhiuzzi A (2013) Promptness and dissipative capacity of MR dampers: experimental investigations. Struct Control Health Monit 20(12):1424–1440. doi:10.1002/stc.1578
18. Caterino N, Spizzuoco M, Occhiuzzi A (2014) Shaking table testing of a steel frame structure equipped with semi-active MR dampers: comparison of control algorithms, Smart Struct Syst, Technopress (in press)
19. Occhiuzzi A (2009) Additional viscous dampers for civil structures: analysis of design methods based on modal damping ratios. Eng Struct 31(5):1093–1101
20. Larsen TJ, Hansen AM (2008) HAWC2 user manual. Risø National Laboratory, Technical University of Denmark, Roskilde, Denmark